Mass and heat transfer resistivities at liquid–vapor interfaces: Beyond the ideal gas

Henning Struchtrup

2025

Original citation:
Struchtrup, H. Mass and heat transfer resistivities at liquid-vapor interfaces: Beyond the ideal gas. *International Journal of Heat and Mass Transfer*, *256*, 127943. https://doi.org/10.1016/j.ijheatmasstransfer.2025.127943

International Journal of Heat and Mass Transfer 256 (2026) 127943

Contents lists available at ScienceDirect

International Journal of Heat and Mass Transfer

journal homepage: www.elsevier.com/locate/hmt

Mass and heat transfer resistivities at liquid–vapor interfaces: Beyond the ideal gas

Henning Struchtrup

Department of Mechanical Engineering, University of Victoria, PO Box 1700 STN CSC, Victoria, V8W 2Y2, British Columbia, Canada

ARTICLE INFO

Keywords:
Liquid–vapor interface
Nonequilibrium
Evaporation
Condensation
Heat transfer
Interface resistivities

ABSTRACT

The classical Hertz–Knudsen–Schrage (HKS) model for non-equilibrium mass and heat transfer across liquid–vapor interfaces is extended to account for real gas effects and non-linearity. Specifically, the HKS relations are re-derived for a temperature and velocity dependent condensation coefficient (Tsuruta et al., 1999) and combined with real gas property relations derived from the Enskog–Vlasov (EV) equation (Struchtrup and Frezzotti, 2022). The resulting non-linear Tsuruta–EV–HKS model is valid for mass and heat transfer up to the critical point. The resulting interfacial resistivities exhibit marked dependence on temperature, with resistivities strongly decreasing towards the critical point, as well as non-linear dependence on mass and heat flux.

1. Introduction

Thermodynamic evaluation shows that non-equilibrium evaporation and heat transfer processes across liquid–vapor interfaces are expected to be accompanied by jumps in temperature and Gibbs free energy, which imply deviation of pressure from saturation [1,2]. The thermodynamic description of these jumps employs a matrix of so-called interfacial resistivities, which link the magnitude of jumps to mass and heat fluxes across the interface. Phenomenological theories of nonequilibrium thermodynamics can only predict the existence of jumps, however, the resistivities must be determined either from experiments or from microscopic modeling.

The study of nonequilibrium processes at interfaces gained renewed interest when Ward and co-workers observed surprisingly large jumps in experiments on the centimeter scale [3,4], which correspondingly predict large resistivities [5,6]. More recent precision experiments show smaller jumps [7].

Since interface coefficients such as resistivities affect processes on the microscale, they are difficult to measure experimentally. Macroscopic experiments suffer from experimental uncertainties that make it almost impossible to verify models, or extract reliable data on transport coefficients [8,9]. As of now, reliable data is not available.

Molecular dynamics (MD) simulations exhibit jumps on the micro- and nano-scale [10,11], but suffer from stochastic noise that strongly affects determination of resistivities [12,13]. To reduce noise, MD simulations are often performed in strong nonequilibrium, and for denser vapors outside the ideal gas regime [11].

There is a rich history of describing interface processes in the kinetic theory of gases, where the vapor is considered as an ideal gas, with a sharp interface at the liquid boundary, and liquid–vapor interaction described by condensation and accommodation coefficients. Best known is the pioneering Hertz–Knudsen model for evaporation mass flux [14,15], which was later improved by Schrage [16]. A complete thermodynamic model requires also an expression for interfacial heat flux which is included in, e.g., [12,13,17–20]. Most, but not all [21,22], kinetic theory models are valid only for small deviations from equilibrium, in particular for vapor velocities well below the speed of sound.

Resistivities can be extracted from such kinetic theory models in dependence of the condensation and accommodation coefficients, thus the difficulty of determining resistivities from experiments or MD simulations is replaced by the equivalent difficulty of extracting these microscopic coefficients.

While in experiments such as Ward's the vapor is expected to be in the ideal gas regime, MD simulations are often conducted closer to the critical point, where real gas effects become important. In this realm, the structure of the interface poses an additional challenge. Indeed, in the highly resolved MD simulations, the interface appears not as a sharp jump in density, but has a diffuse structure where the density decreases continuously from liquid towards vapor. This structure results from the interplay of intermolecular forces, density, and temperature, where MD simulations [11] as well as microscopic modeling [23–25] show wider interfaces at larger temperatures. This variation of interfacial structure affects the overall condensation probability for a particle that leaves the bulk vapor and enters the interfacial zone.

E-mail address: struchtr@uvic.ca.

https://doi.org/10.1016/j.ijheatmasstransfer.2025.127943
Received 28 July 2025; Received in revised form 15 September 2025; Accepted 7 October 2025
Available online 13 October 2025

Tsuruta and co-workers used particle tracking in MD simulations to determine a refined model for the condensation coefficient as function of effective interfacial temperature and the microscopic particle velocity [26,27]. In this model, the condensation probability is higher for faster particles, which can penetrate deeper towards the liquid, but it is lower for higher temperatures, where the interface is wider and vapor density is higher, so that deeper penetration is less likely.

The Tsuruta model was used before to determine interfacial fluxes and resistivities [6,12], where, however, the vapor was still described as an ideal gas, and temperature dependence was not further evaluated. In the present contribution we extend the modeling to account for temperature dependence and real gas effects as well as incorporating non-linearities in the fluxes. To this end, we consider a gas model derived from the Enskog–Vlasov (EV) equation [28,29] which is a modification of the Boltzmann equation [30–32] to account for finite particle size through the Enskog collision term [33] and for the attractive inter-particle potential through the Vlasov force [34].

In the hydrodynamic limit, where the Navier–Stokes–Fourier equations hold, the property relations and transport coefficients of the EV gas are explicitly known, with a van-der-Waals-like thermal equation of state that describes phase equilibrium. With this, the EV gas is a convenient model for this research.

First, combining the kinetic theory modeling in [12] and [13], we derive the non-linear extended Hertz–Knudsen–Schrage (eHKS) model based on the Tsuruta condensation coefficient for the ideal gas. The modeling relies on an approximation of the velocity distribution function that also appears for the EV gas in the hydrodynamic limit [23,24]. This modeling overlap forms the base of extending to the real gas, where, indeed, we model resistivities up to the critical point, in dependence of temperature, and accounting for non-linearities in the fluxes.

While the resulting Tsuruta–EV–eHKS model relies on a number of simplifying assumptions, it accounts for all relevant physics in meaningful approximation, including vanishing resistivities towards the critical point. We believe this model will be useful in particular for a better understanding of MD simulations where real gas effects and non-linearity affect the observations.

The remainder of this paper is structured as follows: Section 2 provides a short introduction of resistivities within the framework of nonequilibrium thermodynamics, where we explicitly include non-linear terms that often are ignored in the literature. In Section 3 we discuss kinetic theory modeling and present the approximate distribution functions for the bulk vapor and the vapor in front of the interface; the Tsuruta condensation coefficient is introduced. This forms the base for the derivation of the non-linear eHKS relations for the Tsuruta model in Section 4. In Section 5 we briefly summarize the EV gas model, which is then combined with the Tsuruta–eHKS model in Section 6, where we show how to obtain the resistivities, and plot these in the linear regime and for the non-linear case. The paper ends with our conclusions.

2. Nonequilibrium thermodynamics: Resistivities

Often the discussion of heat and mass transfer across phase interfaces considers linearized theory which is justified for most but not all applications. For our evaluation of real gas effects in these processes we include processes with large evaporation rates, where Mach number effects cannot be ignored. Thus, we extend the standard model for sharp interfaces in nonequilibrium processes [1,2,6,9] by accounting for non-linear contributions in flow velocity.

As usual in this field, we only consider steady flows normal to the interface, which is at rest in the observer frame, denoting the normal fluxes of mass, momentum, and energy as (J, P, Q). To connect bulk transport equations for adjacent liquid and vapor regions jump relations are needed, which are derived by means of the second law of thermodynamics.

Since the interface does neither produce nor destroy mass, momentum, and energy, the fluxes leaving one phase are equal to those entering the other phase, that is, denoting states of liquid and vapor just at the interface with indices L, V, we have [1,2,6]

$$\begin{aligned} J_L &= J_V = J \\ p_L + \frac{J_L^2}{\rho_L} &= p_V + \frac{J_V^2}{\rho_V} = P \\ J_L\left(h_L + \frac{1}{2}\frac{J^2}{\rho_L^2}\right) + q_L &= J_V\left(h_V + \frac{1}{2}\frac{J^2}{\rho_V^2}\right) + q_V = Q \end{aligned} \tag{1}$$

where p denotes pressure, h is specific enthalpy, and $q_L = -\kappa_L \frac{dT}{dx}|_L$, $q_V = -\kappa_V \frac{dT}{dx}|_V$ are the normal Fourier heat fluxes in the two phases at the interface, with heat conductivity κ; viscous stresses are ignored. The flow velocity is $v = J/\rho$, with the mass density ρ. Fig. 1 provides a simple sketch of geometry, properties, and fluxes.

In nonequilibrium, entropy s is not conserved but must be produced in nonequilibrium processes, hence with direction x pointing from liquid to vapor as in Fig. 1 the entropy balance for the interface reads

$$J s_V + \frac{q_V}{T_V} = J s_L + \frac{q_L}{T_L} + \sigma_S \tag{2}$$

where $\frac{q}{T}$ is the non-convective entropy flux [1,2], and $\sigma_S \geq 0$ is the interfacial entropy generation rate which vanishes in equilibrium and is positive in nonequilibrium.

Eliminating the heat flux in the liquid, q_L, and introducing Gibbs free energy $g = h - Ts$, the entropy generation rate can be written as

$$\sigma_S = \sum_\alpha \mathcal{F}_\alpha \mathcal{J}_\alpha \ , \tag{3}$$

where the entropy generation is interpreted as a sum of products of thermodynamic forces $\mathcal{F}_\alpha$ and thermodynamic fluxes $\mathcal{J}_\alpha$, identified as

$$\mathcal{F} = \left\{ \frac{g_L}{T_L} - \frac{g_V}{T_V} + h_V\left(\frac{1}{T_V} - \frac{1}{T_L}\right) - \frac{1}{2}\frac{J^2}{T_L}\left(\frac{1}{\rho_V^2} - \frac{1}{\rho_L^2}\right), \ \frac{1}{T_V} - \frac{1}{T_L} \right\} \ , \tag{4}$$

$$\mathcal{J} = \left\{ J, \ q_V \right\} \tag{5}$$

In equilibrium the forces (4) as well as the fluxes (5) vanish, thus both phases have the same temperature $T_V = T_L = T$, and identical Gibbs free energies $g_V = g_L$. This is the well known equilibrium condition for coexistence of liquid and vapor [1,35], which states that for given temperature T phase equilibrium is possible only at the saturation pressure $p_{\rm sat}(T)$ with

$$p_L = p_V = p_{\rm sat}(T) \quad \text{and} \quad g_V\left(T, p_{\rm sat}(T)\right) = g_L\left(T, p_{\rm sat}(T)\right) \ . \tag{6}$$

We proceed based on the methods of Linear Irreversible Thermodynamics (LIT) [1,2,36–38]. If a system is in a nonequilibrium state, i.e., the thermodynamic forces are non-zero, thermodynamic fluxes drive the system towards equilibrium. That is, the fluxes are induced by the forces, and must vanish in equilibrium, together with the forces. This behavior is guaranteed by linear relations between fluxes and forces, of the form

$$\mathcal{F}_\alpha = \sum_\beta r_{\alpha\beta} \mathcal{J}_\beta \ , \tag{7}$$

where $r_{\alpha\beta}$ is a matrix of interface resistivities, which is positive semi-definite to ensure non-negative entropy generation σ_S. The matrix is expected to be symmetric to fulfill the Onsager reciprocity relations [1,36]. Phenomenological thermodynamics cannot predict resistivities, which must thus be either found from physical measurements [3,4,7], evaluation of molecular dynamics simulations [5,10,11], or from modeling. The goal of this contribution is to develop models for resistivities by combining ideas from kinetic theory and thermodynamics.

In classical linear irreversible thermodynamics, the resistivities are assumed to depend only on the local temperature, which is either a suitable interface temperature, T_I, or the temperature of the liquid at the interface, T_L. The detailed discussion in Ref. [39] showed that both

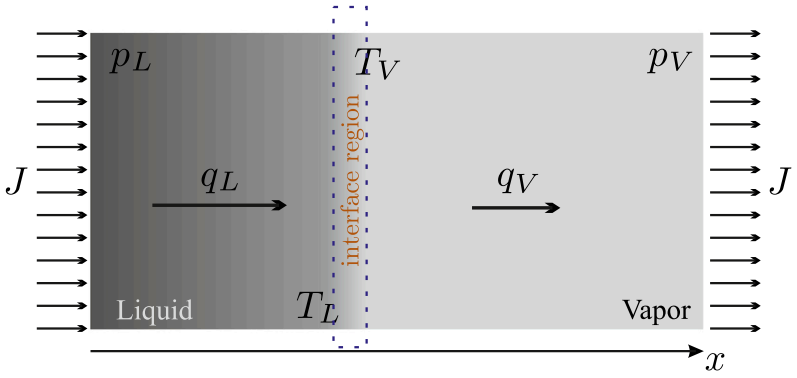

Fig. 1. Geometry, properties, and fluxes in one-dimensional mass and heat transfer across a liquid–vapor interface.

temperatures are expected to be rather close, and in the following we consider the liquid temperature T_L as the relevant temperature for the description of the interface.

Moreover, in Refs. [13,39] we argued that in strong equilibrium the resistivities will depend not only on equilibrium properties — the chosen temperature — but also on the local nonequilibrium state through the fluxes passing the interface, that is $r_{\alpha\beta} = r_{\alpha\beta}\left(T_L, J, q_V\right)$. Then, the linear relations are extended into the non-linear realm—this will be assumed from now on.

Explicitly, the force–flux relations read

$$\begin{bmatrix} \left[\frac{g_L}{T_L} - \frac{g_V}{T_V} + h_V\left(\frac{1}{T_V} - \frac{1}{T_L}\right) - \frac{1}{2}\frac{J^2}{T_L}\left(\frac{1}{\rho_V^2} - \frac{1}{\rho_L^2}\right)\right] \\ \left[\frac{1}{T_V} - \frac{1}{T_L}\right] \end{bmatrix} = \begin{bmatrix} r_{11} & r_{12} \\ r_{21} & r_{22} \end{bmatrix} \begin{bmatrix} J \\ q_V \end{bmatrix} , \quad (8)$$

where non-linearity in the mass flux is explicit in the kinetic energy term in the force, and implicit in the argument of the resistivities. The resistivity matrix must be positive semi-definite, hence $r_{11} \geq 0$, $r_{22} \geq 0$ and $r_{11}\, r_{22} - r_{12}\, r_{21} \geq 0$, symmetry $r_{12} = r_{21}$ is expected.

In the typical linear approach, the non-linearity in the fluxes is not considered, and the kinetic energy contribution does not appear in the mass transfer force. To facilitate comparison with literature results while considering non-linearity, we move this contribution to the other side of the equation, which yields the equivalent form

$$\begin{bmatrix} \left[\frac{g_L}{T_L} - \frac{g_V}{T_V} + h_V\left(\frac{1}{T_V} - \frac{1}{T_L}\right)\right] \\ \left[\frac{1}{T_V} - \frac{1}{T_L}\right] \end{bmatrix} = \begin{bmatrix} r_{11} + \frac{1}{2}\frac{J}{T_L}\left(\frac{1}{\rho_V^2} - \frac{1}{\rho_L^2}\right) & r_{12} \\ r_{21} & r_{22} \end{bmatrix} \begin{bmatrix} J \\ q_V \end{bmatrix} . \quad (9)$$

Here, we recognize a mass-flux-dependent reformulation of the resistivity r_{11}, while now both forces are independent of fluxes. This shift does not change the symmetry properties of the matrix $r_{\alpha\beta}$, and for all cases considered below does not affect its definiteness.

It is generally advantageous to work with dimensionless forces $\hat{\mathcal{F}}_\alpha$, fluxes $\hat{J}$, and resistivities $\hat{r}_{\alpha\beta}$, so that the dimensionless force–flux relations become

$$\begin{bmatrix} \hat{\mathcal{F}}_J \\ \hat{\mathcal{F}}_{q_V} \end{bmatrix} = \begin{bmatrix} \hat{r}_{11} & \hat{r}_{12} \\ \hat{r}_{21} & \hat{r}_{22} \end{bmatrix} \begin{bmatrix} \hat{J} \\ \hat{q}_V \end{bmatrix} . \quad (10)$$

Following Refs. [12,13] we obtain the dimensionless forces through division with the gas constant R of the fluid under consideration or multiplication with temperature T_L, respectively. Introducing temperature in energy units as $\theta = RT$, we thus find

$$\begin{bmatrix} \hat{\mathcal{F}}_J \\ \hat{\mathcal{F}}_{q_V} \end{bmatrix} = \begin{bmatrix} \frac{g_L}{\theta_L} - \frac{g_V}{\theta_V} + h_V\left(\frac{1}{\theta_V} - \frac{1}{\theta_L}\right) \\ \frac{\theta_L}{\theta_V} - 1 \end{bmatrix} . \quad (11)$$

The fluxes are made dimensionless by means of liquid temperature θ_L and the corresponding saturation pressure $p_{\rm sat}\left(\theta_L\right)$,

$$\begin{bmatrix} \hat{J} \\ \hat{q}_V \end{bmatrix} = \begin{bmatrix} \frac{\sqrt{2\pi\theta_L}}{p_{\rm sat}\left(\theta_L\right)} J \\ \frac{\sqrt{2\pi\theta_L}}{p_{\rm sat}\left(\theta_L\right)} \frac{q_V}{\theta_L} \end{bmatrix} ; \quad (12)$$

where the factor $\sqrt{2\pi}$ is suggested by kinetic theory relations that will be seen below.

From these definitions we find the dimensionless resistivities $\hat{r}_{\alpha\beta}$ as

$$\begin{aligned} \hat{r}_{11} &= r_{11}\frac{p_{\rm sat}\left(\theta_L\right)}{R\sqrt{2\pi\theta_L}} + \frac{1}{4\pi}\left[1 - \left(\frac{\rho_V}{\rho_L}\right)^2\right]\left(\frac{p_{\rm sat}\left(\theta_L\right)}{\rho_V\theta_L}\right)^2 \hat{J} , \\ \hat{r}_{12} &= r_{12}\frac{p_{\rm sat}\left(\theta_L\right)\theta_L}{\sqrt{2\pi\theta_L}} , \quad \hat{r}_{21} = r_{21}\frac{p_{\rm sat}\left(\theta_L\right)\theta_L}{\sqrt{2\pi\theta_L}} , \quad \hat{r}_{22} = r_{22}\theta_L^2\frac{p_{\rm sat}\left(\theta_L\right)}{R\sqrt{2\pi\theta_L}} \end{aligned} \quad (13)$$

The kinetic energy correction in $\hat{r}_{11}$ has the sign of the mass flux, hence is positive in evaporation and negative in condensation. It is small compared to r_{11} in all applications considered below where the dimensionless mass flux $\left|\hat{J}\right| \leq 0.4$. In the general non-linear case the dimensionless resistivities are expected to depend on local temperature and the fluxes, that is $\hat{r}_{\alpha\beta}\left(\theta_L, \hat{J}, \hat{q}_V\right)$.

Often one is interested in processes where deviations from equilibrium are small, and the force–flux relations can be linearized. For this, we express the forces to leading order in the deviations from equilibrium

$$\Delta p = p - p_{\rm sat}\left(\theta_L\right) \quad , \quad \Delta\theta = \theta_V - \theta_L . \quad (14)$$

By means of Taylor expansions and thermodynamic property relations $\left(\frac{\partial g}{\partial p}\right)_\theta = \frac{1}{\rho}$, $\left(\frac{\partial g}{\partial T}\right)_p = -s$ [35], the force–flux relations reduce to

$$\begin{bmatrix} -\left[\frac{1}{\rho_{V,\rm sat}} - \frac{1}{\rho_{L,\rm sat}}\right]\frac{\Delta p}{\theta_L} \\ -\frac{\Delta\theta}{\theta_L} \end{bmatrix} = \begin{bmatrix} \hat{r}_{11} & \hat{r}_{12} \\ \hat{r}_{21} & \hat{r}_{22} \end{bmatrix} \begin{bmatrix} \hat{J} \\ \hat{q}_V \end{bmatrix} , \quad (15)$$

where we omitted the arguments of the saturation mass densities $\rho_{V,\rm sat}\left(\theta_L\right)$, $\rho_{L,\rm sat}\left(\theta_L\right)$ for compact notation.

The above equations are valid for general liquid–vapor states. A further simplification results from considering states well below the critical point, where the vapor behaves as an ideal gas, and the specific volume of the liquid can be ignored against the specific volume of the vapor, so that the linearized dimensionless mass transfer force reduces to

$$\hat{\mathcal{F}}_J = -\left[\frac{1}{\rho_{V,\rm sat}} - \frac{1}{\rho_{L,\rm sat}}\right]\frac{\Delta p}{\theta_L} = -\frac{1}{\rho_{V,\rm sat}}\frac{\Delta p}{\theta_L} = -\frac{\Delta p}{p_{\rm sat}\left(\theta_L\right)} . \quad (16)$$

In the following we are mainly interested in non-ideal gas vapors, with relations that will be build as extensions of ideal gas behavior.

3. Kinetic theory models

Evaporation is widely considered in kinetic theory of ideal gases using sharp interface models. Macroscopic interface models derived from kinetic

theory lead to the classical phenomenological Hertz–Knudsen and Schrage formulas, as well as to their refinements [6,12–20]. These models form the base of our extension towards non-ideal gas vapors which will be discussed in later sections.

3.1. Distribution function and moments

In kinetic theory, the behavior of a system of particles (i.e., atoms or molecules) is described by the distribution function f, where $f\left(x_i,t,c_i\right)d\mathbf{c}d\mathbf{x}$ is the number of particles with microscopic velocities in $\{\mathbf{c},\mathbf{c}+d\mathbf{c}\}$ and positions in $\{\mathbf{x},\mathbf{x}+d\mathbf{x}\}$ at time t.

Macroscopic properties such as mass density ρ, momentum density ρv_i, internal energy, pressure tensor, and heat flux can be computed as moments of the distribution function; for comprehensive reviews see [30–32]. Considering only one-dimensional transport normal to the interface, mass density, momentum density (which equals mass flux), and total energy density (that is the sum of internal and kinetic energies) are obtained as

$$\rho = m\int f\,d\mathbf{c}\,, \tag{17}$$

$$\rho v = J = m\int c_n f\,d\mathbf{c}\,, \tag{18}$$

$$\rho\left(\frac{3}{2}\theta+\frac{v^2}{2}\right)=\frac{3}{2}\rho\theta+\frac{1}{2}\frac{J^2}{\rho}=m\int\frac{1}{2}c^2 f\,d\mathbf{c}\,, \tag{19}$$

where m denotes particle mass and $c_n = c_i n_i$ is the velocity component normal to the interface.

Moreover, ignoring viscous stresses, momentum and energy flux are obtained as

$$P = p+\rho v^2 = p+\frac{J^2}{\rho}=m\int c_n^2 f\,d\mathbf{c}\,, \tag{20}$$

$$Q=\rho\left(\frac{5}{2}\theta+\frac{v^2}{2}\right)v+\mathfrak{q}=\left(\frac{5}{2}\rho+\frac{1}{2}\frac{J^2}{\rho^2}\right)J+\mathfrak{q}=m\int\frac{1}{2}c^2c_n f\,d\mathbf{c}\,. \tag{21}$$

Here, $\mathfrak{q}$ denotes the kinetic heat flux for the gas, which as we proceed must be carefully distinguished from the actual heat flux.

In general, the distribution function must be obtained as a solution of the Boltzmann equation. Assuming sufficiently small Knudsen numbers, one finds approximations of the distribution function by means of the Chapman–Enskog (CE) expansion [30–32]. For the one-dimensional flows of interest, we propose the approximation [13]

$$f_{\rm CE}=f_M\left(\rho,\theta,c\right)\left\{1+\frac{c_nJ}{\rho\theta}+\frac{1}{2}\frac{J^2}{\rho^2\theta^2}\left(c_n^2-\theta\right)+\frac{1}{6}\frac{J^3}{\rho^3\theta^3}c_n\left(c_n^2-3\theta\right)+\frac{2}{5}\frac{\mathfrak{q}c_n}{\rho\theta^3}\left(\frac{c^2}{2}-\frac{5}{2}\theta\right)\right\}, \tag{22}$$

where

$$f_{\rm M}\left(\rho,T,c\right)=\frac{\rho}{m}\frac{1}{\left(2\pi\theta\right)^{3/2}}\exp\left(-\frac{c^2}{2\theta}\right)\,. \tag{23}$$

is the Maxwell distribution function in the rest frame of the interface.

Notably, the distribution function $f_{\rm CE}$ produces the proper moments for the conservation laws of mass, momentum, and energy including all non-linear contributions in flow velocity $v = v_n$, that is (17)–(21) are fulfilled. This distribution refines the distribution derived in [12] by including higher order terms in mass flux, which where ignored in [12].

The distribution $f_{\rm CE}$ is well-suited to describe classical bulk flow, as in the Navier–Stokes–Fourier equations. In the vicinity of walls and interfaces, mean free path effects induce Knudsen layer corrections of the distribution [20]. In the following, Knudsen layers are ignored, and the CE distribution is considered to be valid also directly in front of the interface. While this introduces some error into the analysis, the results are still viable for the general understanding of transport behavior across phase interfaces.

We note that when considering interface resistivities, the assumption is that the adjacent bulk phases can be described by the Navier–Stokes–Fourier (NSF) equations of hydrodynamics. This implies that all deviations from (NSF) including Knudsen layers are lumped into the resistivities that describe the jump between the bulk phases.

We will argue in Section 5.3 that the distribution $f_{\rm CE}$(22) is also relevant for non-ideal gases, where the kinetic heat flux q appearing in the distribution is linked to the actual heat flux q through a density dependent factor.

3.2. Vapor distribution at the sharp interface

To develop kinetic theory interface conditions, we assume that the interface is a sharp jump from liquid to vapor, that is we ignore the diffuse structure of the interface, which has a thickness of ~10−20 particle diameters [11,24]. The discussion below is closely following Ref. [12], with some changes in notation.

When a particle from the vapor phase hits the liquid–vapor interface, it interacts with the liquid particles. Depending upon the microscopic conditions for the particular interaction, the particle can be absorbed by the liquid — it condenses — or it might be reflected back into the vapor. The energy of the liquid particles at the interface fluctuates, and occasionally a particle gains enough energy to leave the liquid to enter the vapor—the particle evaporates.

Evaporation, condensation and reflection processes influence the distribution function at the interface and determine the rates of mass and energy transfer across the interface. We write the distribution function directly at the interface as

$$f_{\rm int}=\begin{cases} f_{\rm in}, & c_n'<0\\ f_{\rm em}, & c_n>0\end{cases}\,, \tag{24}$$

where $f_{\rm in}$ is the distribution of incident particles, and $f_{\rm em}$ is the distribution of emitted particles; the prime at the velocity of incident particles simplifies to distinguish between incident and emitted particles.

The distribution of particles leaving the interface is the sum of a term that describes evaporation, and a term that describes the reflection of non-condensing particles back into the vapor. The relation between the incident and emitted distribution functions is written as [40,41],

$$f_{\rm em}=\chi_e\left(c_k\right)f_{\rm M}\left(\rho_{\rm sat}\left(\theta_L\right),\theta_L,c\right)+\frac{1}{\left|c_n\right|}\int_{c_n'<0}f_{\rm in}\left(c_k'\right)R_c\left(c_k'\to c_k\right)\left|c_n'\right|d\mathbf{c}'\,. \tag{25}$$

Here, $\chi_e\left(c_k\right)$ is the evaporation probability, which in general must be assumed to depend on particle velocity relative to the interface, and $R_c\left(c_k'\to c_k\right)$ is the condensation–reflection kernel, which gives the probability that a particle that hits the interface with velocities in $\left\{c_k',c_k'+dc'\right\}$ will be scattered with velocities in $\left\{c_k,c_k+dc\right\}$ [30]. The liquid side of the interface is assumed to be in local equilibrium [6, 19,41,42], and thus the distribution of evaporating particles is linked to the Maxwellian distribution $f_{\rm M}\left(\rho_{\rm sat}\left(\theta_L\right),\theta_L,c\right)$, where θ_L is the liquid surface temperature and $\rho_{\rm sat}\left(\theta_L\right)$ is the corresponding saturation density.

In the classical Maxwell wall reflection kernel, it is assumed that a portion γ of particles is reflected diffusively, that is in a Maxwell distribution in equilibrium with the wall, and the portion $(1-\gamma)$ is reflected specularly, where γ is the so-called accommodation coefficient [30,31]. While specular reflection can easily be included in liquid–vapor interface models [12], in the following we adapt the Maxwell model to evaporation assuming that non-condensing particles return into the vapor by diffuse reflection only, that is $\gamma = 1$. Indeed, a vapor particle entering the interfacial region will interact with several particles before either entering the liquid as a condensed particle, or returning to the vapor as a reflected particle, while specular reflections appear to be unlikely.

Following Ref. [12], but with $\gamma = 1$, we consider the, properly normalized, condensation–reflection kernel

$$R_c\left(c_k'\to c_k\right)=\alpha\left(c_k'\right)\frac{\alpha\left(-c_k\right)\left|c_n\right|f_0\left(\theta_L,c\right)}{\int_{c_n>0}\alpha\left(-c_k\right)\left|c_n\right|f_0\left(\theta_L,c\right)d\mathbf{c}}\,, \tag{26}$$

where, $\alpha\left(c_k'\right) = 1 - \chi_c(c_k')$ is the reflection probability, $\chi_c(c_k')$ is the condensation coefficient, and

$$f_0\left(\theta_L, c\right) = \frac{m}{\rho}\sqrt{\frac{\theta_L}{2\pi}} f_M\left(\theta_L, c\right) = \frac{1}{2\pi\theta_L^2}\exp\left(-\frac{c^2}{2\theta_L}\right) \tag{27}$$

is the reduced Maxwellian at θ_L. The reflection kernel fulfills the reciprocity relation [30,40,41,43],

$$|c_n'|\, f_0\left(\theta_L, c'\right) R_c\left(c_k' \to c_k\right) = |c_n|\, f_0\left(\theta_L, c\right) R_c\left(-c_k \to -c_k'\right) \ . \tag{28}$$

In thermal equilibrium no net evaporation or condensation occurs, the vapor and the liquid have the same temperatures, $\theta_V = \theta_L$, the vapor pressure is equal to the saturation pressure, $p = p_{\rm sat}(\theta_L)$, and the vapor is in the corresponding Maxwellian distribution $f_M\left(\rho_{\rm sat}\left(\theta_L\right), \theta_L, c\right)$. This equilibrium behavior is guaranteed by the micro-reversibility condition [42],

$$f_{\rm in}|_{eq} = f_{\rm em}|_{eq} = f_M\left(\rho_{\rm sat}\left(\theta_L\right), \theta_L, c\right) \ . \tag{29}$$

Combining (25), (26), (29) and using that

$$f_0\left(\theta_L, c\right)\ f_{\rm M}\left(\rho_{\rm sat}\left(\theta_L\right), \theta_L, c'\right) = f_{\rm M}\left(\rho_{\rm sat}\left(\theta_L\right), \theta_L, c\right)\ f_0\left(\theta_L, c'\right) \tag{30}$$

the micro-reversibility condition reduces to

$$1 = \chi_e\left(c_k\right) + \alpha\left(c_k\right) \quad \Rightarrow \quad \chi_e\left(c_k\right) = 1 - \alpha\left(c_k\right) = \chi_c(c_k)\ , \tag{31}$$

that is microscopic evaporation and condensation coefficients agree.

As stated before, we shall in the following consider the Chapman–Enskog distribution $f_{\rm CE}$ as the distribution of incident particles. Thus, combining the above, kinetic theory interface conditions will be determined from the distribution function

$$f_{\rm int} = \begin{cases} f_{\rm CE}, & c_n' < 0 \\ f_{\rm em}, & c_n > 0 \end{cases} \ , \tag{32}$$

where the distribution of particles leaving the interface is given by

$$f_{\rm em} = \chi_c\left(c_k\right) f_{\rm M}\left(\rho_{\rm sat}\left(\theta_L\right), \theta_L, c\right) + \left[1 - \chi_c\left(-c_k\right)\right] \Lambda f_0\left(\theta_L, c\right) \tag{33}$$

with the abbreviation

$$\Lambda = \frac{\int_{c_n'<0}\left[1 - \chi_c\left(c_k'\right)\right]|c_n'|\, f_{\rm CE}\left(c_k'\right) d\mathbf{c}'}{\int_{c_n>0}\left[1 - \chi_c\left(-c_k\right)\right]|c_n|\, f_0\left(\theta_L, c\right) d\mathbf{c}} \ . \tag{34}$$

3.3. Condensation coefficient

To proceed, we require meaningful expressions for the condensation coefficient $\chi_c\left(c_k\right)$. In kinetic theory of ideal gases one typically assumes the condensation coefficient as a constant with value close to unity. A more elaborate model was suggested by Tsuruta and co-workers based on tracking particles in molecular dynamics simulations [26,27]. Based on their data for argon-like particles they suggested a velocity dependent condensation coefficient of the form

$$\chi_c\left(c_n'\right) = \psi\left[1 - \omega\exp\left(-\frac{c_n'^2}{2\theta_L}\right)\right] \ . \tag{35}$$

This condensation probability depends on the normal impact velocity c_n'. In this model, faster particles are more likely to condense, since they can more easily penetrate towards the liquid and dissipate their energy to a larger number of neighboring particles. The dimensionless coefficients ψ, ω that describe the details of the condensation probability depend on the temperature of the liquid [26], with data given in Table 1 for actual argon temperatures, as well as temperatures relative to the critical temperature $\theta_{\rm cr}$, i.e. $\theta_L/\theta_{\rm cr}$, where $\theta_{\rm cr} \simeq 150$K.

Fig. 2 shows the data points relative to polynomial fits of second order over the temperature ratio $\theta_L/\theta_{\rm cr}$. These fits will be used in the following.

Classical kinetic theory models with constant condensation coefficient for ideal gas vapors arise from setting $\omega = 0$. The data in Fig. 2 shows that for temperatures well below the critical point the coefficient ψ is close to unity while ω is rather small. With this, the Tsuruta model agrees well with the typical assumptions in classical kinetic theory for lower temperatures. Closer to the critical point, however, the Tsuruta model predicts significantly smaller coefficient ψ and larger ω, and thus marked decrease of the overall condensation coefficient χ_c. This behavior might be explained by the changing thickness of the diffuse interfacial region, which is rather narrow for lower temperatures, where liquid and vapor densities differ strongly, while it becomes wider towards the critical point, where liquid and vapor densities differ less.

In the following our interest lies in processes at higher temperatures, where non-ideal gas behavior becomes relevant. We consider the Tsuruta model as viable for the description of the condensation probability.

Table 1
Temperature dependent coefficients in the Tsuruta model as functions of temperature θ_L and relative to critical temperature [26,27].

T_L/K	$\theta_L/\theta_{\rm cr}$	ψ	ω
84	0.56	0.971	0.086
90	0.60	0.935	0.220
102	0.68	0.923	0.299
120	0.80	0.75	0.388
130	0.867	0.685	0.554

4. Extended Hertz–Knudsen–Schrage equations

With the kinetic theory description of the previous section, we have all that is required to determine non-equilibrium interface conditions. These result from the requirement that the fluxes of mass and energy as determined from the interface distribution $f_{\rm int}$ (32) and from the bulk distribution at the interface $f_{\rm CE}$(22) agree. Specifically we consider the equations

$$m\int c_n f_{\rm CE} d\mathbf{c} = m\int c_n f_{\rm int} d\mathbf{c} \tag{36}$$

$$m\int\left(\frac{1}{2}c^2 c_n - \frac{5}{2}\theta\right) c_n f_{\rm CE} d\mathbf{c} = m\int\left(\frac{1}{2}c^2 c_n - \frac{5}{2}\theta\right) c_n f_{\rm int} d\mathbf{c} \tag{37}$$

which through the distribution function $f_{\rm CE}$ (22) are linear in the kinetic heat flux $\mathfrak{q}$, but non-linear in the mass flux J. The resulting equations are the extension of the well-known Hertz–Knudsen–Schrage (HKS) equations [6,13–16] towards non-linearity.

Wolfram Mathematica was used for the evaluation of these equations. The resulting expressions are rather lengthy, even more so with the Tsuruta condensation coefficient (35), and were stored and further evaluated on the computer.

In order to give the reader some idea of the results, we present HKS equations for special cases, in particular for constant condensation coefficient $\chi_c = \psi$, and for the linear case with the Tsuruta model.

As for the LIT expression, we use the saturation state at liquid temperature to define the dimensionless fluxes

$$\hat{J} = J\frac{\sqrt{2\pi\theta_L}}{p_{\rm sat}\left(\theta_L\right)} \quad , \quad \hat{\mathfrak{q}}_V = \frac{\mathfrak{q}_V}{\theta_L}\frac{\sqrt{2\pi\theta_L}}{p_{\rm sat}\left(\theta_L\right)} \ . \tag{38}$$

Furthermore, we denote the ratio between vapor and liquid temperatures as

$$\Theta = \frac{\theta_V}{\theta_L} \ . \tag{39}$$

4.1. eHKS model for constant condensation coefficient

With constant condensation coefficient $\chi_c = \psi$ we find mass and kinetic heat flux at the interface as

$$\hat{J} = \frac{2\psi}{2-\psi}\left[\frac{\rho_{V,\rm sat}\theta_L}{p_{\rm sat}} - \frac{\rho_V\theta_L}{p_{\rm sat}}\sqrt{\Theta} - \frac{1}{4\pi}\frac{p_{\rm sat}}{\rho_V\theta_L}\frac{\hat{J}^2}{\sqrt{\Theta}}\right] \ , \tag{40}$$

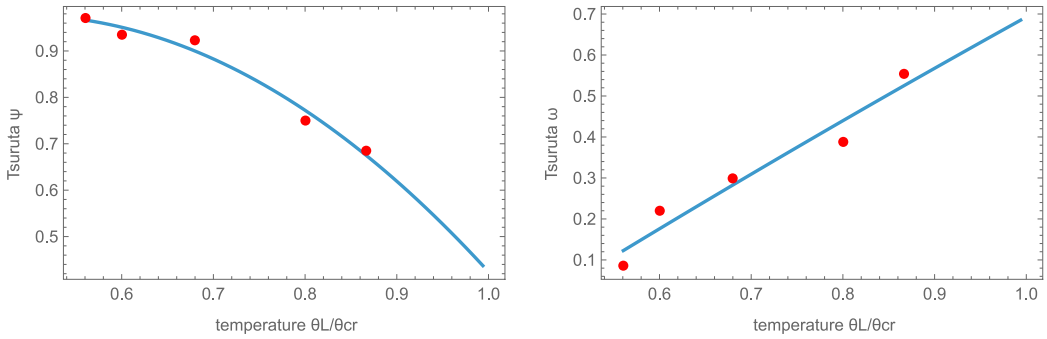

Fig. 2. Tsuruta coefficients as functions of temperature ratio θ_L/θ_{cr}.

$$\hat{q}_V = \frac{2\psi}{2-\psi}\left(2-\frac{5}{2}\Theta\right)\left[\frac{\rho_{V,sat}\theta_L}{p_{sat}} - \frac{\rho_V\theta_L}{p_{sat}}\sqrt{\Theta}\right] + 4\frac{\rho_V\theta_L}{p_{sat}}\left[1-\Theta\right]\sqrt{\Theta}$$
$$+\frac{1}{4\pi}\left[8\frac{1-\psi}{2-\psi}\left(\frac{\rho_V\theta_L}{p_{sat}}\sqrt{\Theta}\left(1-\frac{7}{4}\Theta\right)+\frac{1}{2}\frac{\rho_{V,sat}\theta_L}{p_{sat}}\Theta\right)\right.$$
$$\left.-\Theta\left(\frac{\rho_V\theta_L}{p_{sat}}\sqrt{\Theta}+2\frac{\rho_{V,sat}\theta_L}{p_{sat}}\right)\right]\frac{p_{sat}^2}{\rho_V^2\theta_L^2}\frac{\hat{J}^2}{\Theta}$$
$$+\frac{1}{8\pi^2}\frac{\psi}{2-\psi}\frac{p_{sat}^3}{\rho_V^3\theta_L^3}\frac{\hat{J}^4}{\sqrt{\Theta}}\,, \tag{41}$$

where for compact notation we abbreviated $p_{sat} = p_{sat}(\theta_L)$, $\rho_{V,sat} = \rho_{V,sat}(\theta_L)$.

These equations were presented in Ref. [13], only that here we set the accommodation coefficient γ to unity, and — in preparation for the extension to non-ideal gas vapors — explicitly write mass densities, instead of employing the ideal gas law and writing pressures. Indeed, if the vapor behaves as an ideal gas, then saturation pressure and vapor pressure are related to densities as $p_{sat} = \rho_{V,sat}\theta_L$, and $p_V = \rho_V\theta_V = \rho_V\theta_L\Theta$, respectively, and the HKS equations assume the dimensionless form given in Ref. [13].

4.2. Linear Tsuruta-eHKS model

Next, we consider the HKS equations for the Tsuruta condensation coefficient in the linear limit. Ignoring non-linear contributions in the mass flow, evaluating (36) we find expressions for mass and kinetic heat flux that are linear in the vapor densities, and can be written as

$$J = \sqrt{\frac{\theta_L}{2\pi}}\alpha_{sat}(\theta_L,\theta_V)\,\rho_{V,sat} - \sqrt{\frac{\theta_L}{2\pi}}\alpha_V(\theta_L,\theta_V)\,\rho_V \tag{42}$$

$$q_V = \theta_L\sqrt{\frac{\theta_L}{2\pi}}\beta_{sat}(\theta_L,\theta_V)\,\rho_{V,sat} - \theta_L\sqrt{\frac{\theta_L}{2\pi}}\beta_V(\theta_L,\theta_V)\,\rho_V \tag{43}$$

Here, α_{sat}, α_V, β_{sat}, β_V are dimensionless coefficients. Aiming for linear relations, we set $\theta_V = \theta_L + \Delta\theta$ and linearize the coefficients in $\Delta\theta$ as

$$\alpha_{sat}(\theta_L,\theta_V) = \alpha_0 + \alpha_{1,sat}\frac{\Delta\theta}{\theta_L}\,, \tag{44}$$
$$\alpha_V(\theta_L,\theta_V) = \alpha_0 + \alpha_{1,V}\frac{\Delta\theta}{\theta_L}\,, \tag{45}$$
$$\beta_{sat}(\theta_L,\theta_V) = \beta_0 + \beta_{1,sat}\frac{\Delta\theta}{\theta_L}\,, \tag{46}$$
$$\beta_V(\theta_L,\theta_V) = \beta_0 + \beta_{1,V}\frac{\Delta\theta}{\theta_L}\,. \tag{47}$$

The coefficients α_0, $\alpha_{1,sat}$, $\alpha_{1,V}$, β_0, $\beta_{1,sat}$, $\beta_{1,V}$ depend on the two temperature-dependent coefficients Tsuruta coefficients $\psi(\theta_L)$, $\omega(\theta_L)$ through explicit but lengthy polynomial expressions that can be found in Appendix, Eqs. (A.1)–(A.7).

Furthermore, we linearize in the density deviation

$$\Delta\rho = \rho_V - \rho_{V,sat}\,, \tag{48}$$

keeping only linear terms in $\Delta\rho$, $\Delta\theta$, to find the dimensionless linear Tsuruta–HKS equations as

$$\hat{J} = -\alpha_0\frac{\Delta\rho}{p_{sat}/\theta_L} + (\alpha_{1,sat}-\alpha_{1,V})\frac{\rho_{V,sat}\theta_L}{p_{sat}}\frac{\Delta\theta}{\theta_L}\,, \tag{49}$$
$$\hat{q}_V = -\beta_0\frac{\Delta\rho}{p_{sat}/\theta_L} + (\beta_{1,sat}-\beta_{1,V})\frac{\rho_{V,sat}\theta_L}{p_{sat}}\frac{\Delta\theta}{\theta_L}\,. \tag{50}$$

For the classical case with $\omega = 0$ the coefficients reduce to

$$\alpha_0 = \frac{2\psi}{2-\psi}\quad,\quad \alpha_{1,sat} = 0\quad,\quad \alpha_{1,V} = \frac{\psi}{2-\psi}\,, \tag{51}$$
$$\hat{\beta}_0 = -\frac{\psi}{2-\psi}\quad,\quad \beta_{1,sat} = -\frac{5\psi}{2-\psi}\quad,\quad \beta_{1,V} = \frac{1}{2-\psi}\left(8-\frac{19}{2}\psi\right) \tag{52}$$

which give the linearized classical HKS relations as

$$\hat{J} = \frac{\psi}{2-\psi}\left[-\frac{\Delta\rho}{p_{sat}/\theta_L} - \frac{1}{2}\frac{\rho_{V,sat}\theta_L}{p_{sat}}\frac{\Delta\theta}{\theta_L}\right]\,, \tag{53}$$
$$\hat{q}_V = \frac{\psi}{2-\psi}\frac{\Delta\rho}{p_{sat}/\theta_L} - \frac{8-\frac{9}{2}\psi}{2-\psi}\frac{\rho_{V,sat}\theta_L}{p_{sat}}\frac{\Delta\theta}{\theta_L}\,. \tag{54}$$

4.3. Non-linear Tsuruta-HKS model

For the non-linear case with Tsuruta model, the corresponding equations were explicitly determined on the computer, where they were subsequently evaluated as explained further below. Due to their length, the equations are not shown in detail. The expressions for dimensionless mass and kinetic heat flux can be written in compact form, with $\Theta = \theta_V/\theta_L$, as

$$\hat{J} = \mathsf{J}(\rho_V,\Theta,\hat{J};\theta_L) \qquad \hat{q}_V = \mathsf{Q}(\rho_V,\Theta,\hat{J};\theta_L)\,. \tag{55}$$

where θ_L appears as a parameter that determines the values of $\rho_{V,sat}(\theta_L)$, $p_{sat}(\theta_L)$, $\psi(\theta_L)$, $\omega(\theta_L)$ which appear in the functions J and Q.

For the classical case, $\omega = 0$, these equations reduce to (40), (41), and when linearized, they reduce to (49), (50) with the coefficients (A.1)–(A.7).

5. Enskog-Vlasov model for non-ideal gas

The Enskog–Vlasov non-ideal gas model results from evaluation of the Enskog–Vlasov (EV) equation [28,29], which is an extension of the Boltzmann equation that accounts for the finite size of particles through the Enskog collision term for hard spheres [33], and for the attractive force between particles through the Vlasov model [34]. Similar to the van-der-Waals-gas, the property relations for the EV gas are valid for liquid and vapor phases, with saturation states determined from

Maxwell's equal area argument [35]. Here we only list the relevant thermodynamic properties for this model, with details and further references found in Refs. [23,24].

5.1. Property relations

As in the cited references, we consider a unit system in which particle diameter a, particle mass m and potential parameter ϕ_a are set to unity, $a = m = \phi_a = 1$. The van-der-Waals-like thermal equation of state relates pressure, mass density and temperature as

$$p(\rho,\theta) = \rho\theta\left(1+\frac{2\pi}{3}\rho Y\right) - \frac{2\pi}{3}\chi_1\rho^2 \,, \tag{56}$$

where Y denotes the pair correlation function for which we use the expression proposed by Carnahan and Starling [44],

$$Y(\rho) = \frac{1}{2}\frac{2-\frac{\pi}{6}\rho}{\left(1-\frac{\pi}{6}\rho\right)^3} \,. \tag{57}$$

The parameter χ_1 arises through the Vlasov force, for attractive power potentials of order ϖ it is found as $\chi_1 = \frac{\varpi}{\varpi-3}$; we will use $\varpi = 6$, hence $\chi_1 = 2$.

Specific internal energy u and enthalpy h of the EV gas are given by

$$u(\rho,\theta) = \frac{3}{2}\theta - \frac{2\pi}{3}\chi_1\rho \quad , \quad h = u + \frac{p}{\rho} = \left(\frac{5}{2}+\frac{2\pi}{3}\rho Y\right)\theta - \frac{4\pi}{3}\chi_1\rho \,. \tag{58}$$

The corresponding entropy follows from integration of the Gibbs equation $\theta ds = du - \frac{p}{\rho^2}d\rho$ as

$$s - s_0 = \frac{3}{2}\ln\frac{\theta}{\theta_0} - \ln\frac{\rho}{\rho_0} - \left[\frac{3-\frac{\pi}{3}\frac{a^3}{m}\rho}{\left(1-\frac{\pi}{6}\frac{a^3}{m}\rho\right)^2} - \frac{3-\frac{\pi}{3}\frac{a^3}{m}\rho_0}{\left(1-\frac{\pi}{6}\frac{a^3}{m}\rho_0\right)^2}\right] \tag{59}$$

where s_0, ρ_0, θ_0 define a suitable reference state that cancels from the equations below.

With the definition of the Gibbs free energy, $g = h - \theta s$, the (dimensionless) driving force for mass transfer $(11)_1$ results from considering these relations for liquid and vapor as

$$\begin{aligned}\hat{\mathcal{F}}_J &= \frac{g_L}{\theta_L} - \frac{g_V}{\theta_V} + h_V\left(\frac{1}{\theta_V}-\frac{1}{\theta_L}\right) = \frac{5}{2}\left(1-\frac{\theta_V}{\theta_L}\right) - \frac{3}{2}\ln\frac{\theta_L}{\theta_V} + \ln\frac{\rho_L}{\rho_V} \\ &+\frac{2\pi}{3}\left[\rho_L Y_L - \rho_V Y_V\frac{\theta_V}{\theta_L}\right] - \frac{4\pi}{3}\chi_1\frac{\rho_L-\rho_V}{\theta_L} \\ &+\left[\frac{3-\frac{\pi}{3}\rho_L}{\left(1-\frac{\pi}{6}\rho_L\right)^2} - \frac{3-\frac{\pi}{3}\rho_V}{\left(1-\frac{\pi}{6}\rho_V\right)^2}\right] ,\end{aligned} \tag{60}$$

where we abbreviated $Y_L = Y(\rho_L)$, $Y_V = Y(\rho_V)$.

The heat transfer force $(11)_2$

$$\hat{\mathcal{F}}_{q_V} = \frac{\theta_L}{\theta_V} - 1 \tag{61}$$

is independent of the property relations.

5.2. Phase equilibrium

In phase equilibrium both forces vanish, $\hat{\mathcal{F}}_J = \hat{\mathcal{F}}_{q_V} = 0$, hence $\theta_V = \theta_L = \theta$, and the saturation densities of liquid and vapor, $\rho_{L,\mathrm{sat}}(\theta)$, $\rho_{V,\mathrm{sat}}(\theta)$, are related as

$$\begin{aligned}0 &= \ln\frac{\rho_{L,\mathrm{sat}}}{\rho_{V,\mathrm{sat}}} + \frac{2\pi}{3}\left[\rho_{L,\mathrm{sat}}Y_{L,\mathrm{sat}} - \rho_{V,\mathrm{sat}}Y_{V,\mathrm{sat}}\right] - \frac{4\pi}{3}\chi_1\frac{\rho_{L,\mathrm{sat}}-\rho_{V,\mathrm{sat}}}{\theta} \\ &+\left[\frac{3-\frac{\pi}{3}\rho_{L,\mathrm{sat}}}{\left(1-\frac{\pi}{6}\rho_{L,\mathrm{sat}}\right)^2} - \frac{3-\frac{\pi}{3}\rho_{V,\mathrm{sat}}}{\left(1-\frac{\pi}{6}\rho_{V,\mathrm{sat}}\right)^2}\right] ,\end{aligned} \tag{62}$$

which is equivalent to the result of the equal area evaluation as outlined in [23,24]. The saturation pressure is

$$p_{\mathrm{sat}}(\theta) = p\left(\rho_{L,\mathrm{sat}}(\theta),\theta\right) = p\left(\rho_{V,\mathrm{sat}}(\theta),\theta\right) \,. \tag{63}$$

Fig. 3 shows saturation pressure and mass densities as functions of temperature for values up to the critical point, for which

$$\theta_{\mathrm{cr}} = 0.7456 \quad , \quad p_{\mathrm{cr}} = 0.06748 \quad , \quad \rho_{\mathrm{cr}} = 0.2491 \,. \tag{64}$$

Saturation data was determined numerically.

5.3. Actual and kinetic heat flux

Evaluating the Enskog–Vlasov equation and its moment equations in the Navier–Stokes–Fourier limit [24,45], one identifies Fourier's law for the kinetic heat flux as (in one dimension)

$$\mathfrak{q}^{(\mathrm{NSF})} = -\frac{15}{4}\sqrt{\theta}\frac{\left(1+\frac{3}{5}\frac{2\pi}{3}\rho Y\right)}{\frac{16}{5}\sqrt{\pi}Y}\frac{d\theta}{dx} \,, \tag{65}$$

and the actual heat flux as

$$q^{(\mathrm{NSF})} = -\left[\frac{15}{4}\sqrt{\theta}\frac{\left(1+\frac{3}{5}\frac{2\pi}{3}\rho Y\right)^2}{\frac{16}{5}\sqrt{\pi}Y} + \frac{2}{3}\sqrt{\pi}\sqrt{\theta}\rho^2 Y\right]\frac{d\theta}{dx} \,. \tag{66}$$

Eliminating the temperature gradient we find an explicit relation between actual and kinetic heat fluxes as

$$q = \mathcal{G}(\rho)\,\mathfrak{q} \,, \tag{67}$$

with a factor that depends only on mass density,

$$\mathcal{G}(\rho) = 1 + \frac{3}{5}\frac{2\pi}{3}\rho Y + \frac{128}{225}\pi\frac{\rho^2 Y^2}{1+\frac{2\pi}{5}\rho Y} \,. \tag{68}$$

This relation is valid without restriction, that is it can be applied to liquid and vapor states. In the ideal gas limit vapor density is negligibly small and $\mathcal{G} \to 1$, so that kinetic and actual heat flux agree.

5.4. Useful relations

Below we require derivatives of the equation of state that we list here for convenience.

The thermal equation of state (56) gives the derivatives of pressure with respect to density and temperature as

$$\left(\frac{\partial p}{\partial\rho}\right)_\theta = \theta\left(1+\frac{2\pi}{3}\rho Y\right) + \frac{2\pi}{3}\rho\theta\left(Y+\rho\frac{dY}{d\rho}\right) - \frac{4\pi}{3}\chi_1\rho \,, \tag{69}$$

$$\left(\frac{\partial p}{\partial\theta}\right)_\rho = \rho\left(1+\frac{2\pi}{3}\rho Y\right) \,, \tag{70}$$

where

$$\frac{dY}{d\rho} = \frac{\pi}{36}\frac{15-\pi\rho}{\left(1-\frac{\pi}{6}\rho\right)^4} \,. \tag{71}$$

From standard relations between thermodynamic properties [35] we thus find the derivatives of density as

$$\left(\frac{\partial\rho_V}{\partial p}\right)_{\theta_L} = \frac{1}{\left(\frac{\partial p}{\partial\rho}\right)_{\theta_L}} = \frac{1}{\theta\left(1+\frac{2\pi}{3}\rho Y\right) + \frac{2\pi}{3}\rho\theta\left(Y+\rho\frac{dY}{d\rho}\right) - \frac{4\pi}{3}\chi_1\rho} \,, \tag{72}$$

$$\left(\frac{\partial\rho}{\partial\theta}\right)_p = -\frac{\left(\frac{\partial p}{\partial\theta}\right)_\rho}{\left(\frac{\partial p}{\partial\rho}\right)_\theta} = -\frac{\rho\left(1+\frac{2\pi}{3}\rho Y\right)}{\theta\left(1+\frac{2\pi}{3}\rho Y\right) + \frac{2\pi}{3}\rho\theta\left(Y+\rho\frac{dY}{d\rho}\right) - \frac{4\pi}{3}\chi_1\rho} \,. \tag{73}$$

6. Resistivities for non-ideal gas vapors

We now combine the kinetic theory based eHKS model for interfacial fluxes, incorporating the Tsuruta condensation coefficient, with the non-ideal Enskog–Vlasov gas model, and extract the resistivities as functions of temperature up to the critical point. This procedure

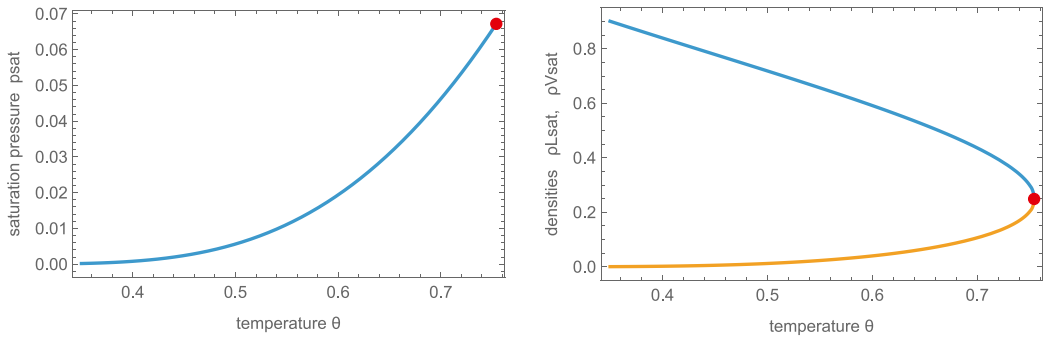

Fig. 3. Saturation pressure $p_{\rm sat}\,(\theta)$ and saturation densities $\rho_{L,{\rm sat}}\,(\theta)$, $\rho_{V,{\rm sat}}\,(\theta)$ of the EV gas as functions of temperature. The dot indicates the critical point.

relies on the distribution function $f_{\rm CE}$ that was used in determining the eHKS relations being written in terms of the mass densities and temperatures of the vapor and the kinetic heat flux, which all are meaningful for the EV gas as well. This allows us to use the van-der-Waals-like pressure (56) and other equations of state of the EV gas, and the relation between actual and kinetic heat fluxes, to extend the ideal gas eHKS relations towards the non-ideal gas case. The Tsuruta condensation coefficient was determined for the case of non-ideal gas vapor, hence is meaningful in particular in this realm.

Below, the linear case, where resistivities depend only on the local temperature θ_L, and the non-linear case, where resistivities depend on temperature and fluxes, are treated separately.

6.1. Linear resistivities $\hat{r}_{\alpha\beta}\,(\theta_L)$

In the linear case, resistivities connect the fluxes $\hat{J}$, $\hat{q}_V$ to pressure and temperature deviations, Δp, $\Delta\theta$ as expressed in Eq. (15). In the linear Tsuruta–HKS equations (49), (50) the fluxes are related to density and temperature deviations, $\Delta\rho$, $\Delta\theta$. Thus, to extract the resistivities from the linear HKS equations, we express the density variation $\Delta\rho$ through pressure and temperature variation by expanding the equation of state,

$$\Delta\rho = \rho_V - \rho_{V,{\rm sat}}\,(\theta_L) = \left(\frac{\partial\rho_V}{\partial p}\right)_{\theta_L,{\rm sat}} \Delta p + \left(\frac{\partial\rho_V}{\partial\theta}\right)_{p,{\rm sat}} \Delta\theta\ . \tag{74}$$

where the explicit density derivatives are given in (72), (73). With this, the Tsuruta–EV–HKS equations read

$$\hat{J} = -\alpha_0\left[\theta_L\left(\frac{\partial\rho_V}{\partial p}\right)_{\theta_L,{\rm sat}}\right]\frac{\Delta p}{p_{\rm sat}} + \left[\alpha_{1,{\rm sat}} - \alpha_{1,V} - \alpha_0\left[\frac{\theta_L}{\rho_{V,{\rm sat}}}\left(\frac{\partial\rho_V}{\partial\theta}\right)_{p,{\rm sat}}\right]\right]\frac{\rho_{V,{\rm sat}}\theta_L}{p_{\rm sat}}\frac{\Delta\theta}{\theta_L}\ , \tag{75}$$

$$\hat{\rm q}_V = -\beta_0\left[\theta_L\left(\frac{\partial\rho_V}{\partial p}\right)_{\theta_L,{\rm sat}}\right]\frac{\Delta p}{p_{\rm sat}} + \left[\beta_{1,{\rm sat}} - \beta_{1,V} - \beta_0\left[\frac{\theta_L}{\rho_{V,{\rm sat}}}\left(\frac{\partial\rho_V}{\partial\theta}\right)_{p,{\rm sat}}\right]\right]\frac{\rho_{V,{\rm sat}}\theta_L}{p_{\rm sat}}\frac{\Delta\theta}{\theta_L}\ . \tag{76}$$

For comparison with (15), we introduce the linearized thermodynamic force by writing

$$\frac{\Delta p}{p_{\rm sat}} = -\mathcal{A}\left[-\left(\frac{1}{\rho_{V,{\rm sat}}} - \frac{1}{\rho_{L,{\rm sat}}}\right)\frac{\Delta p}{\theta_L}\right] \quad\Longrightarrow\quad \mathcal{A} = \frac{\theta_L/p_{\rm sat}}{\frac{1}{\rho_{V,{\rm sat}}} - \frac{1}{\rho_{L,{\rm sat}}}}\ , \tag{77}$$

and we replace the kinetic heat flux $\hat{\rm q}_V$ with the actual heat flux $\hat{q}_V$ by means of (67). With this, the equations can be written as

$$\begin{bmatrix}\hat{J}\\ \hat{q}_V\end{bmatrix} = \hat{L}_{\alpha\beta}\begin{bmatrix}-\left(\frac{1}{\rho_{V,{\rm sat}}} - \frac{1}{\rho_{L,{\rm sat}}}\right)\frac{\Delta p}{\theta_L}\\ -\frac{\Delta\theta}{\theta_L}\end{bmatrix}, \tag{78}$$

with the dimensionless Onsager matrix

$$\hat{L}_{\alpha\beta} = \begin{bmatrix}\alpha_0\left[\mathcal{A}\theta_L\left(\frac{\partial\rho_V}{\partial p}\right)_{\theta_L,{\rm sat}}\right] & \left[\alpha_{1,V} - \alpha_{1,{\rm sat}} + \alpha_0\left(\frac{\theta_L}{\rho_{V,{\rm sat}}}\left(\frac{\partial\rho_V}{\partial\theta}\right)_{p,{\rm sat}}\right)\right]\left[\frac{\rho_{V,{\rm sat}}\theta_L}{p_{\rm sat}}\right]\\ \beta_0\left[\mathcal{G}_{\rm sat}\mathcal{A}\theta_L\left(\frac{\partial\rho_V}{\partial p}\right)_{\theta_L,{\rm sat}}\right] & \left[\beta_{1,V} - \beta_{1,{\rm sat}} + \beta_0\left(\frac{\theta_L}{\rho_{V,{\rm sat}}}\left(\frac{\partial\rho_V}{\partial\theta}\right)_{p,{\rm sat}}\right)\right]\left[\mathcal{G}_{\rm sat}\frac{\rho_{V,{\rm sat}}\theta_L}{p_{\rm sat}}\right]\end{bmatrix}. \tag{79}$$

Here, $\mathcal{G}_{\rm sat} = \mathcal{G}\left(\rho_{V,{\rm sat}}\,(\theta_L)\right)$ is evaluated at the saturation state of the vapor.

Inversion of the Onsager matrix finally yields the desired matrix of resistivities for the linear case,

$$\hat{r}_{\alpha\beta}\,(\theta_L) = \hat{L}^{-1}_{\alpha\beta}\ . \tag{80}$$

Fig. 4 shows the resulting resistivities for the Tsuruta–EV–HKS model in blue, in comparison to the Tsuruta–HKS model for the ideal gas, for which

$$\theta\left(\frac{\partial\rho}{\partial p}\right)_\theta = \theta\frac{1}{\theta} = 1 \quad,\quad \frac{\theta}{\rho}\left(\frac{\partial\rho}{\partial\theta}\right)_p = \frac{\theta}{\rho}\left(-\frac{p}{\theta^2}\right) = -1 \quad,\quad \mathcal{A} = \mathcal{G}_{\rm sat} = 1\ . \tag{81}$$

All Tsuruta–EV resistivities for the real gas (blue) decrease with temperature and vanish towards the critical point. Considering that at the critical point the differences of liquid and vapor — and thus the interface — vanish, this behavior is physically meaningful. It must be noted that the Tsuruta condensation coefficient (35) was not determined up to the critical point, hence these results rely on extrapolation, see Fig. 2.

The contrast to the ideal gas case (orange) is most striking for $\hat{r}_{11}$ which for the ideal gas case grows strongly with temperature, but decreases for the real gas case. While the modeling yields symmetric resistivities $\hat{r}_{12} = \hat{r}_{21}$ for the ideal gas case, the real gas effects lead to asymmetry. Considering the simplicity of the modeling approach, the relatively weak asymmetry is not very concerning. Nevertheless, more refined modeling approaches should be developed in the future.

6.2. Non-linear resistivities $\hat{r}_{\alpha\beta}\,(\theta_L, \hat{J})$, $\hat{r}_{\alpha\beta}\,(\theta_L, \hat{q}_V)$

For the non-linear case, to link the non-linear Tsuruta–eHKS relations (55) to the force–flux relations of nonequilibrium thermodynamics (10), we rewrite the latter in terms of the kinetic heat flux, so that

$$\begin{bmatrix}\hat{F}_J\\ \hat{F}_{q_V}\end{bmatrix} = \begin{bmatrix}\hat{r}_{11} & \hat{r}_{12}\\ \hat{r}_{21} & \hat{r}_{22}\end{bmatrix}\begin{bmatrix}\hat{J}\\ \mathcal{G}(\rho)\,\hat{\rm q}_V\end{bmatrix}\ . \tag{82}$$

As is often done [10,11,24,46], we consider single flux cases, where either $\hat{q}_V = \mathcal{G}(\rho)\,\hat{\rm q}_V = 0$ for pure evaporation, or $\hat{J} = 0$ for pure heat

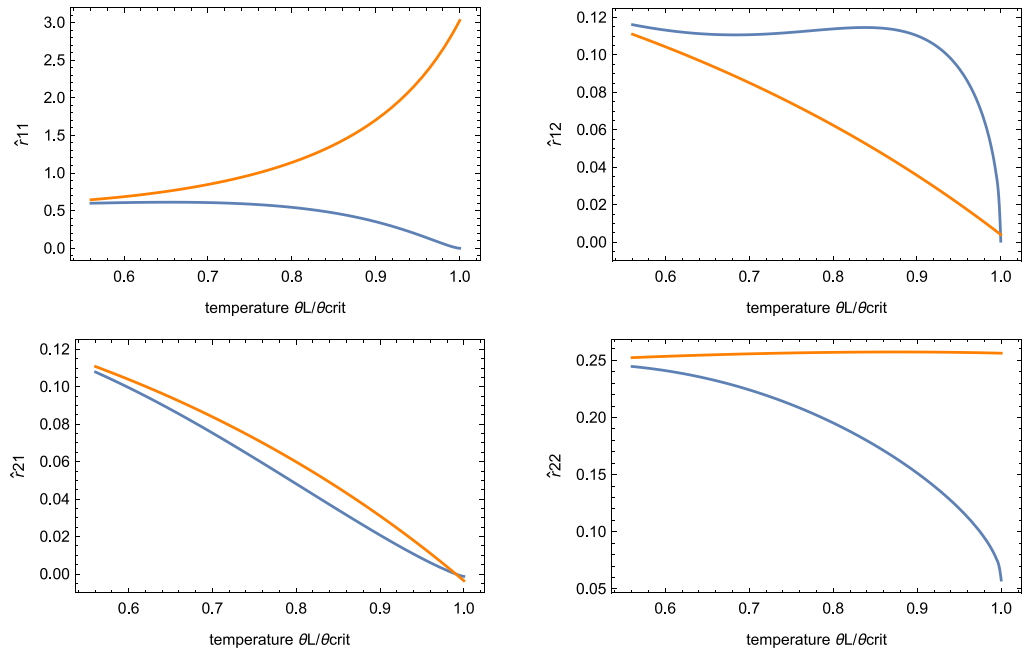

Fig. 4. Blue: Resistivities $\hat{r}_{\alpha\beta}\left(\theta_L\right)$ for the Tsuruta–EV–HKS model in the linear case as function of relative temperature θ_L/θ_{cr} up to the critical point ($\theta_{cr} = 0.7546$). Orange: Ideal gas resistivities $\hat{r}_{\alpha\beta}\left(\theta_L\right)$ for the Tsuruta condensation coefficient. (For interpretation of the references to color in this figure legend, the reader is referred to the web version of this article.)

transfer. The resistivities for these case are determined from

$$\text{Evaporation:} \quad \hat{r}_{11} = \frac{\hat{\mathcal{F}}_J}{\hat{J}} \quad , \quad \hat{r}_{21} = \frac{\hat{\mathcal{F}}_{q_V}}{\hat{J}} \, , \qquad \text{with } \hat{\mathrm{q}}_V = 0 \quad (83)$$

$$\text{Heat transfer:} \quad \hat{r}_{12} = \frac{\hat{\mathcal{F}}_J}{\mathcal{G}(\rho)\,\hat{\mathrm{q}}_V} \quad , \quad \hat{r}_{22} = \frac{\hat{\mathcal{F}}_{q_V}}{\mathcal{G}(\rho)\,\hat{\mathrm{q}}_V} \, , \qquad \text{with } \hat{J} = 0 \quad (84)$$

To proceed, we consider the liquid temperature as the main variable, that is prescribe θ_L, and determine the other quantities. Specifically, the evaluation requires the thermodynamic forces (60), (61) for the EV gas, which we can write formally as

$$\hat{\mathcal{F}}_J = \hat{\mathsf{F}}_J\left(\rho_V, \rho_L, \Theta; \theta_L\right) \quad , \quad \hat{\mathcal{F}}_{q_V} = \hat{\mathsf{F}}_{q_V}\left(\rho_V, \rho_L, \Theta; \theta_L\right) \, , \qquad (85)$$

and the kinetic theory HKS conditions for the Tsuruta model (55)

$$\hat{J} = \mathsf{J}\left(\rho_V, \Theta, \hat{J}; \theta_L\right) \qquad \hat{\mathrm{q}}_V = \mathsf{Q}\left(\rho_V, \Theta, \hat{J}; \theta_L\right) \, . \qquad (86)$$

Moreover, temperatures and mass densities of the phases, and, for non-linear processes the mass flux, are related through the conservation law for momentum $(1)_2$, which in dimensionless form reads

$$\frac{p\left(\rho_L, \theta_L\right)}{p_{\text{sat}}} + \frac{p_{\text{sat}}/\theta_L}{\rho_L}\frac{\hat{J}^2}{2\pi} = \frac{p\left(\rho_V, \theta_V\right)}{p_{\text{sat}}} + \frac{p_{\text{sat}}/\theta_L}{\rho_V}\frac{\hat{J}^2}{2\pi} \, . \qquad (87)$$

For the evaporation case ($\hat{q}_V = 0$) we perform the following steps:

1. Prescribe a value for liquid interface temperature θ_L.
2. Prescribe a value for mass flux $\hat{J}$.
3. Determine corresponding vapor mass density ρ_V and temperature ratio $\Theta = \theta_V/\theta_L$ from the eHKS equations $\hat{J} = \mathsf{J}\left(\rho_V, \Theta, \hat{J}; \theta_L\right)$, $0 = \mathsf{Q}\left(\rho_V, \Theta, \hat{J}; \theta_L\right)$.
4. Determine the corresponding liquid mass density ρ_L from conservation of momentum (87).
5. Determine the corresponding forces $\hat{\mathcal{F}}_J$ and $\hat{\mathcal{F}}_{q_V}$ from (85).
6. Finally, use the collected data to determine the resistivities $\hat{r}_{11}$ and $\hat{r}_{21}$ from (83).

This procedure mimics experiments and molecular simulations, where one would control mass flux through pressure [3,4,10,11]. With liquid temperature θ_L and mass flux $\hat{J}$ as controlled variables, we list and plot the results for the resistivities as

$$\text{Evaporation:} \ \hat{r}_{11}\left(\theta_L, \hat{J}\right) \quad , \quad \hat{r}_{21}\left(\theta_L, \hat{J}\right) \, . \qquad (88)$$

The corresponding procedure to find the resistivities $\hat{r}_{12}$ and $\hat{r}_{22}$ for pure heat transfer is similar, only that in Step 2 vapor temperature ratio $\Theta = \theta_V/\theta_L$ is prescribed instead of mass flux, and in Step 3 vapor density ρ_V is obtained from $0 = \mathsf{J}\left(\rho_V, \Theta, 0; \theta_L\right)$, and with that kinetic heat flux from $\hat{\mathrm{q}}_V = \mathsf{Q}\left(\rho_V, \Theta, 0; \theta_L\right)$. This yields the resistivities as functions of temperature and heat flux $\hat{q}_V = \mathcal{G}\left(\rho_V\right)\hat{\mathrm{q}}_V$,

$$\text{Heat transfer:} \ \hat{r}_{12}\left(\theta_L, \hat{q}_V\right) \quad , \quad \hat{r}_{22}\left(\theta_L, \hat{q}_V\right) \, . \qquad (89)$$

The four resistivities are depicted in Fig. 5 as functions of temperature and their relevant flux. While their temperature dependence shows the same principal behavior as in the linear case, non-linear influence of the fluxes is clearly visible, in particular for the evaporation resistivities ($\hat{r}_{11}$, $\hat{r}_{21}$).

Towards the critical temperature the mass transfer resistivity $\hat{r}_{11}$ drops sharply, reaching values of zero for forced condensation, where $\hat{J} < 0$, already for temperatures θ_L below the critical point.

The exact determination of resistivities from experiments or molecular simulations is rather difficult due to significant errors caused by experimental uncertainty or stochastic noise [3,4,9–13]. At present there is no meaningful data available for evaluation of the combined temperature and flux dependence of resistivities.

For general non-linear processes with mass and heat flux present, the relation (82) between forces and the HKS relations provide only two relations for four resistivities $\hat{r}_{\alpha\beta}\left(\theta_L, \hat{J}, \hat{q}_V\right)$, thus the system is underdetermined. While meaningful functions $\hat{r}_{\alpha\beta}\left(\theta_L, \hat{J}, \hat{q}_V\right)$ can be obtained from optimization [13], these are not unique and thus have limited physical meaning. Non-linear resistivities provide an excellent means of data visualization for single-flux cases, where they are unique, but might be difficult to explore in the general two-flux case, due to the inherent non-uniqueness.

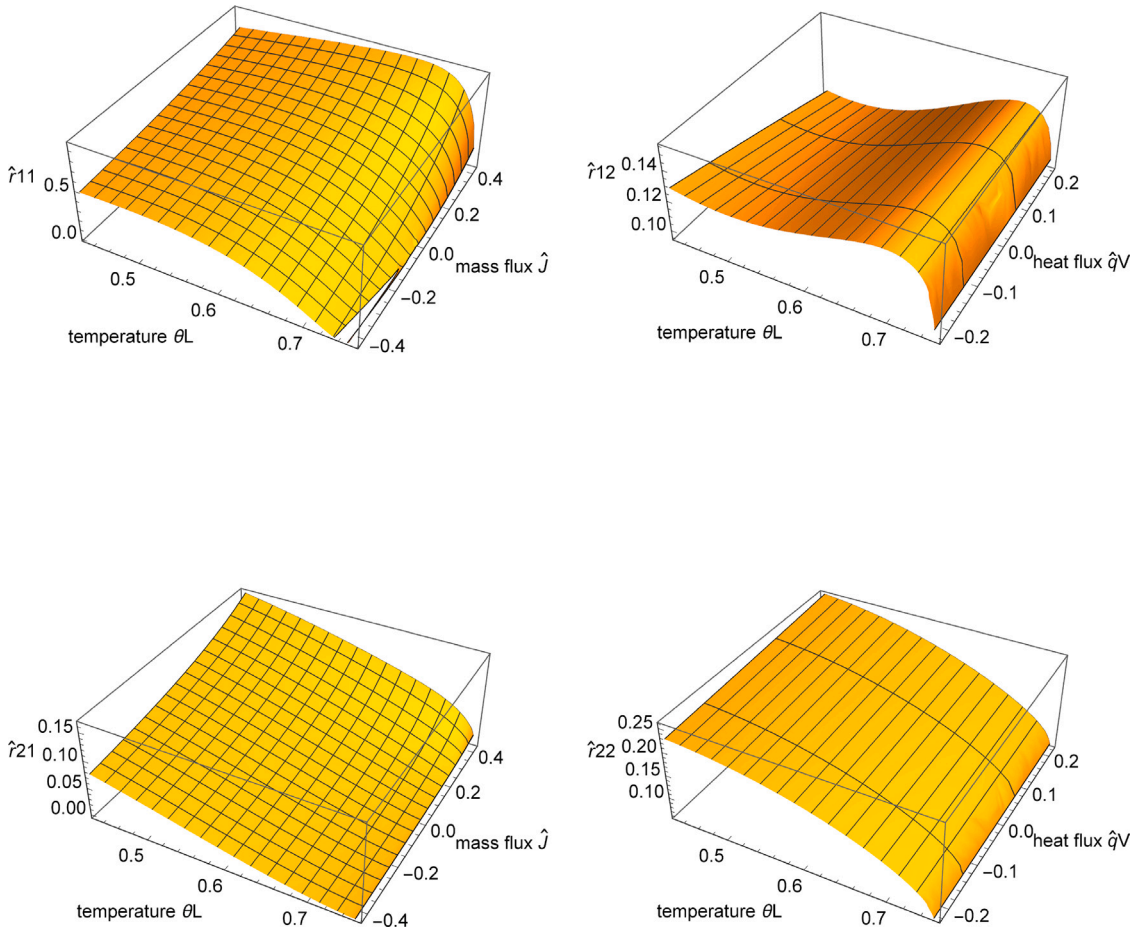

Fig. 5. Resistivities $\hat{r}_{\alpha\beta}$ for the Tsuruta–EV–HKS model as functions of temperature and mass flux $\hat{J}$ (for $\hat{r}_{11}$, $\hat{r}_{21}$) or heat flux $\hat{q}_V$ (for $\hat{r}_{12}$, $\hat{r}_{22}$).

6.3. Resistivities from molecular dynamics

Accurate resistivity data from experiments or microscopic simulations is scarce, hence a detailed comparison of the modeling results with data is not possible. At present, the most thorough data available might be the recent MD simulations by Homes and Vrabec [11]. In order to obtain reliable data with little noise, MD simulations are often run at large fluxes, where non-linear effects play a role. In [13] we evaluated the Homes–Vrabec data with emphasis on non-linear effects, while now we are more interested in temperature dependence, in particular changes as the temperature approaches the critical temperature.

Fig. 6 shows the dimensionless resistivities (13) as computed from the original data [11] as functions of relative temperature θ_L/θ_{cr}, where the relative size of mass and heat fluxes is indicated by gray levels, with points darker for larger absolute fluxes. The largest temperatures are $\sim 0.83\,\theta_{cr}$, hence the temperatures are below the region where in Fig. 5 resistivities are strongly decreasing.

As discussed in [13], the values of resistivities from MD are affected by the assumed location of the interface to which data curves are extrapolated, which accounts for the observed lack of symmetry of the resistivity matrix. Moreover, due to stochastic noise effects, the data scatters relatively widely, in particular for smaller fluxes, but nevertheless some trends are clearly visible as follows:

At least for large mass fluxes, the resistivity $\hat{r}_{11}$ is a slowly decreasing function of temperature, in agreement with Fig. 5. The heat transfer resistivity $\hat{r}_{22}$ exhibits comparatively faster decrease, which as well agrees with Fig. 5. Both off-diagonal resistivities decrease rather weakly with increasing temperature, with $\hat{r}_{21}$ appearing to be larger for larger mass fluxes, which also agrees with Fig. 5.

7. Conclusions

Combining ideas of nonequilibrium thermodynamics and kinetic theory of ideal and non-ideal gases, we have derived the non-linear Tsuruta–EV–eHKS model for mass and heat transfer across liquid–vapor interfaces, which generalizes the classical Hertz–Knudsen–Schrage (HKS) model for non-ideal gas vapor up to the critical point, as well as extending it to account for non-linearities due to Mach number effects. Real gas effects are included through the use of the EV gas model for liquid and vapor, and through the Tsuruta condensation coefficient which accounts for temperature dependence and particle impact velocity. The corresponding matrix of interface resistivities for heat and mass transfer was determined, where all resistivities show marked decrease as temperature increases towards the critical point, as well as clear variations due to non-linearity. This stands in contrast to classical kinetic theory results which rely on constant condensation coefficients and ideal gas behavior to find constant values for the dimensionless resistivities.

Due to the inherent difficulty of determining resistivities from physical experiments or molecular simulations, a detailed comparison of model predictions with data from other sources is presently not possible. Thus, this paper aims to extend the knowledge about interface coefficients in general, but not at providing a detailed model for practical applications. Nevertheless, evaluation of MD data shows a general agreement of trends.

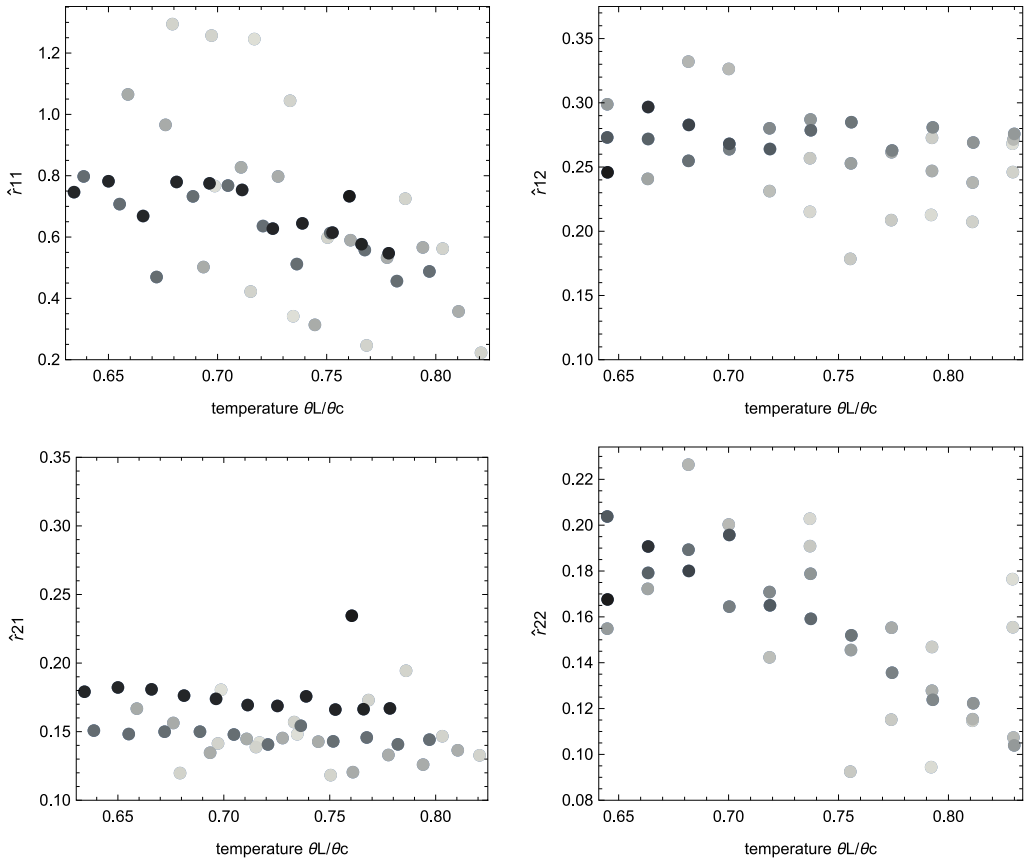

Fig. 6. Dimensionless resistivities $\hat{r}_{\alpha\beta}$ determined from MD simulations by Homes and Vrabec [11] plotted over relative temperature $\theta_{\mathrm{L}}/\theta_{\mathrm{cr}}$. The gray level indicates the strength of dimensionless mass and heat flux, respectively, with darker colors indicating larger absolute fluxes. Dimensionless mass fluxes are in $\hat{J} = \{0, \ldots, 0.5\}$ and heat fluxes in $\hat{q}_V = \{-0.08, \ldots, 0\}$.

In summary, we strongly believe that the observed behavior — marked temperature dependence, in particular for temperatures approaching the critical point, and non-linearity — will affect experiments and molecular dynamics simulations, and recommend careful consideration of these effects in evaluation of the resulting data. Useful data of high quality could, e.g., be obtained from kinetic models based on the Enskog–Vlasov equation which allow deterministic solutions for flows close and far from equilibrium and can be tuned to agree with Lennard-Jones gases [47,48].

Declaration of competing interest

The authors declare the following financial interests/personal relationships which may be considered as potential competing interests: Henning Struchtrup reports financial support was provided by Natural Sciences and Engineering Research Council of Canada.

Acknowledgments

The author wishes to thank Prof. Aldo Frezzotti (Milano, Italy) for helpful discussions and suggestions, and Simon Homes and Jadran Vrabec (TU Berlin, Germany) for providing their detailed Molecular Dynamics data from Ref. 11. This work was supported by the Natural Sciences and Engineering Research Council of Canada (NSERC) through Discovery Grant RGPIN-2022-03188.

Appendix. Coefficients for linear Tsuruta-HKS

Here we list the explicit expressions for the coefficients α_0, $\alpha_{1,\mathrm{sat}}$, $\alpha_{1,V}$, β_0, $\beta_{1,\mathrm{sat}}$, $\beta_{1,V}$, that appear in the linearized Tsuruta–HKS model.

With the abbreviation

$$\zeta = 80\,(2-\psi)\,(1-\psi) + \left(80+23\sqrt{2}\right)\psi\omega - \left(40+23\sqrt{2}\right)\psi^2\omega + 13\sqrt{2}\psi^2\omega^2\ . \tag{A.1}$$

we find the coefficients as

$$\alpha_0 = \frac{\psi}{\zeta}\left[160\,(1-\psi) + 80\,(2\psi-1)\,\omega - \left(40-3\sqrt{2}\right)\psi\omega^2\right] \tag{A.2}$$

$$\alpha_{1,\mathrm{sat}} = -\frac{75\psi^2}{\sqrt{2}\zeta^2}\,[2-2\psi+\psi\omega]\left[\left(4+\sqrt{2}\right)\psi\omega^3 - 16\psi\omega^2 + 8\psi\omega + 12\omega^2 - 8\omega\right]\ , \tag{A.3}$$

$$\begin{aligned}\alpha_{1,V} = \frac{\psi}{\zeta^2}\Big[&6400\,(2-\psi)\,(1-\psi)^2 + 3840\sqrt{2}\omega \\ &+ \left(12800-7160\sqrt{2}\right)\psi\omega \\ &- \left(19200-2800\sqrt{2}\right)\psi^2\omega + \left(1104+3180\sqrt{2}\right)\psi\omega^2 \\ &+ \left(992-1760\sqrt{2}\right)\psi^2\omega^2 \\ &+ \left(1095+330\sqrt{2}\right)\psi^2\omega^3 + \left(6400+520\sqrt{2}\right)\psi^3\omega \\ &- \left(496+1420\sqrt{2}\right)\psi^3\omega^2 \\ &- \left(1095-880\sqrt{2}\right)\psi^3\omega^3 + \left(276-150\sqrt{2}\right)\psi^3\omega^4\Big]\ ,\end{aligned} \tag{A.4}$$

$$\hat{\beta}_0 = \frac{10}{\zeta}\left[-80\psi\,(1-\psi) + 120\psi\omega - 160\psi^2\omega + \left(40+10\sqrt{2}\right)\psi^2\omega^2\right]\ ,$$

(A.5)

$$\beta_{1,\mathrm{sat}} = \frac{10}{\zeta^2}\Big[-3200\psi(2-\psi)(1-\psi)^2 + 3200\psi\omega - \left(14400+950\sqrt{2}\right)\psi^2\omega + \left(3200+385\sqrt{2}\right)\psi^2\omega^2 + \left(16000+1900\sqrt{2}\right)\psi^3\omega - \left(6400\psi^3\omega^2+1855\sqrt{2}\right)\psi^3\omega^2 + \left(773+490\sqrt{2}\right)\psi^3\omega^3 - \left(4800+950\sqrt{2}\right)\psi^4\omega + \left(2400+1470\sqrt{2}\right)\psi^4\omega^2 - \left(373+795\sqrt{2}\right)\psi^4\omega^3 - \left(12-145\sqrt{2}\right)\psi^4\omega^4\Big], \quad (A.6)$$

$$\beta_{1,V} = \frac{10}{\zeta^2}\Big[320(2-\psi)(1-\psi)^2(16-19\psi) + \left(14080+2752\sqrt{2}\right)\psi\omega - \left(37120+7922\sqrt{2}\right)\psi^2\omega + \left(6448+3405\sqrt{2}\right)\psi^2\omega^2 + \left(31040+7588\sqrt{2}\right)\psi^3\omega - \left(10336+6529\sqrt{2}\right)\psi^3\omega^2 + \left(1188+1318\sqrt{2}\right)\psi^3\omega^3 - \left(8000+2418\sqrt{2}\right)\psi^4\omega + \left(3648+3124\sqrt{2}\right)\psi^4\omega^2 - \left(788+1261\sqrt{2}\right)\psi^4\omega^3 + \left(105+145\sqrt{2}\right)\psi^4\omega^4\Big] \quad (A.7)$$

Data availability

Data will be made available on request.

References

[1] S. Kjelstrup, D. Bedeaux, Non-Equilibrium Thermodynamics of Heterogeneous Systems, World Scientific, 2008, http://dx.doi.org/10.1142/6672.

[2] H. Struchtrup, A Thermodynamic Introduction To Transport Phenomena, Springer Cham, 2024, http://dx.doi.org/10.1007/978-3-031-61868-0.

[3] G. Fang, C.A. Ward, Temperature measured close to the interface of an evaporating liquid, Phys. Rev. E 59 (1999) 417–428, http://dx.doi.org/10.1103/PhysRevE.59.417.

[4] M.A. Kazemi, C.A. Ward, Assessment of the statistical rate theory expression for evaporation mass flux, Int. J. Heat Mass Trans. 179 (2021) 121709, http://dx.doi.org/10.1016/j.ijheatmasstransfer.2021.121709.

[5] D. Bedeaux, S. Kjelstrup, Transfer coefficients for evaporation, Phys. A 270 (1999) 413–426, http://dx.doi.org/10.1016/S0378-4371(99)00162-4.

[6] M. Bond, H. Struchtrup, Mean evaporation and condensation coefficients based on energy dependent condensation probability, Phys. Rev. E 70 (2004) 061605, http://dx.doi.org/10.1103/PhysRevE.70.061605.

[7] E.Ya. Gatapova, Evaporation into half-space: Experiments with water at the molecular mean free path scale, Phys. Fluids 36 (2024) 091707, http://dx.doi.org/10.1063/5.0228893.

[8] R. Marek, J. Straub, Analysis of the evaporation coefficient and the condensation coefficient of water, Int. J. Heat Mass Trans. 44 (2001) 39–53, http://dx.doi.org/10.1016/S0017-9310(00)00086-7.

[9] M.T. Rauter, A. Aasen, S. Kjelstrup, Ø. Wilhelmsen, A comparative study of experiments and theories on steady-state evaporation of water, Chem. Thermodyn. Therm. Anal. 8 (2023) 100091, http://dx.doi.org/10.1016/j.ctta.2022.100091.

[10] J. Xu, S. Kjelstrup, D. Bedeaux, A. Røsjorde, L. Rekvig, Verification of Onsager's reciprocal relations for evaporation and condensation using non-equilibrium molecular dynamics, J. Colloid Interface Sci. 299 (2006) 452–463, http://dx.doi.org/10.1016/j.jcis.2006.01.043.

[11] S. Homes, J. Vrabec, Resistivities across the vapor–liquid interface of a simple fluid: An assessment of methods, Phys. Fluids 36 (2024) 022122, http://dx.doi.org/10.1063/5.0193522.

[12] J.P. Caputa, H. Struchtrup, Interface model for non-equilibrium evaporation, Phys. A 390 (2011) 31–42, http://dx.doi.org/10.1016/j.physa.2010.09.019.

[13] P. Feyzi Oskouei, H. Struchtrup, Nonlinear mass and heat transfer across liquid-vapor interfaces, Phys. Rev. E 112 (2025) 025501, http://dx.doi.org/10.1103/wzz4-d6sg.

[14] H. Hertz, Über die Verdunstung der Flüssigkeiten, insbesondere des Quecksilbers, im luftleeren Raume, Ann. Phys., Lpz. 253 (10) (1882) 177–193, http://dx.doi.org/10.1002/andp.18822531002.

[15] M. Knudsen, Die maximale Verdampfungsgeschwindigkeit des Quecksilbers, Ann. Phys., Lpz. 352 (13) (1915) 697–708, http://dx.doi.org/10.1002/andp.19153521306.

[16] R.W. Schrage, A Theoretical Study of Interphase Mass Transfer, Columbia University Press, New York, 1953, http://dx.doi.org/10.7312/schr90162.

[17] Y.P. Pao, Application of kinetic theory to the problem of evaporation and condensation, Phys. Fluids 14 (1971) 306–312, http://dx.doi.org/10.1063/1.1693429.

[18] Y.P. Pao, Temperature and density jumps in the kinetic theory of gases and vapors, Phys. Fluids 14 (1971) 1340–1346, http://dx.doi.org/10.1063/1.1693612.

[19] J.W. Cipolla, H. Lang, S.K. Loyalka, Kinetic theory of condensation and evaporation. II, J. Chem. Phys. 61 (1974) 69–77, http://dx.doi.org/10.1063/1.1681672.

[20] Y. Sone, Y. Onishi, Kinetic theory of evaporation and condensation—Hydrodynamic equation and slip boundary condition, J. Phys. Soc. Japan 44 (1978) 1981–1994, http://dx.doi.org/10.1143/JPSJ.44.1981.

[21] T. Ytrehus, S. Østmo, Kinetic theory approach to interphase processes, Int. J. Multiph. Flow 22 (1996) 133–155, http://dx.doi.org/10.1016/0301-9322(95)00056-9.

[22] C. Cercignani, Strong evaporation of a polyatomic gas, in: 12th International Symposium on Rarefied Gas Dynamics; Technical Papers, Part 1, American Institute of Aeronautics and Astronautics, New York, 1981, pp. 305–320.

[23] H. Struchtrup, A. Frezzotti, Twenty-six moment equations for the Enskog-Vlasov equation, J. Fluid Mech. 940 (2022) A–40, http://dx.doi.org/10.1017/jfm.2022.98.

[24] H. Struchtrup, H. Jahandideh, A. Couteau, A. Frezzotti, Heat transfer and evaporation processes from the Enskog-Vlasov equation, and its moment equations, Int. J. Heat Mass Transfer 223 (2024) 125238, http://dx.doi.org/10.1016/j.ijheatmasstransfer.2024.125238.

[25] R. Bhattacharjee, H. Struchtrup, A. Singh Rana, Temperature dependent korteweg stress coefficient from the Enskog–Vlasov equation, Phys. Fluids 36 (2024) 122139, http://dx.doi.org/10.1063/5.0244649.

[26] T. Tsuruta, H. Tanaka, T. Masuoka, Condensation/evaporation coefficient and velocity distributions at liquid–vapor interface, Int. J. Heat Mass Trans. 42 (1999) 4107–4116, http://dx.doi.org/10.1016/S0017-9310(99)00081-2.

[27] G. Nagayama, T. Tsuruta, A general expression for the condensation coefficient based on transition state theory and molecular dynamics simulation, J. Chem. Phys. 118 (2003) 1392–1399, http://dx.doi.org/10.1063/1.1528192.

[28] L. de Sobrino, On the kinetic theory of a van der Waals gas, Can. J. Phys. 45 (1967) 363–385, http://dx.doi.org/10.1139/p67-035.

[29] M. Grmela, Kinetic equation approach to phase transitions, J. Stat. Phys. 3 (1971) 347–364, http://dx.doi.org/10.1007/BF01011389.

[30] C. Cercignani, Theory and Application of the Boltzmann Equation, Scottish Academic Press, Edinburgh, 1975.

[31] H. Struchtrup, Macroscopic Transport Equations for Rarefied Gas Flows, Springer, Berlin, 2005, http://dx.doi.org/10.1007/3-540-32386-4.

[32] G.M. Kremer, An Introduction To the Boltzmann Equation and Transport Processes in Gases, Springer, Berlin Heidelberg, 2010, http://dx.doi.org/10.1007/978-3-642-11696-4.

[33] D. Enskog, The numerical calculation of phenomena in fairly dense gases, Ark. Mat. Astr. Fys. 16 (1921) 1–60.

[34] A.A. Vlasov, Many-Particle Theory and Its Application To Plasma, Gordon and Breach, 1961.

[35] H. Struchtrup, Thermodynamics and Energy Conversion—Second Edition, Springer, Heidelberg, 2024, http://dx.doi.org/10.1007/978-3-031-60556-7.

[36] S.R. de Groot, P. Mazur, Non-Equilibrium Thermodynamics, Dover Publications, New York, 1984.

[37] D. Bedeaux, Nonequilibrium thermodynamics and statistical physics of surfaces, Adv. Chem. Phys. 64 (1986) 47, http://dx.doi.org/10.1002/9780470142882.ch2.

[38] D.C. Venerus, H.C. Öttinger, A Modern Course in Transport Phenomena, Cambridge University Press, Cambridge, 2018, http://dx.doi.org/10.1017/9781316416174.

[39] H. Struchtrup, H.C. Öttinger, Nonequilibrium liquid-vapor interfaces: Linear and nonlinear descriptions, Phys. Rev. E 108 (2023) 064801.

[40] F. Sharipov, Onsager-Casimir reciprocity relations for open gaseous systems at arbitrary rarefaction: I. General theory for single gas, Phys. A 203 (1994) 437–456, http://dx.doi.org/10.1016/0378-4371(94)90009-4.

[41] I. Kuščer, M. Robnik, Semi-microscopic description of evaporation and condensation, J. Phys. A: Math. Gen. 13 (1980) 621–627, http://dx.doi.org/10.1088/0305-4470/13/2/025.

[42] K.W. Kolasinski, Surface Science, Wiley, Hoboken, 2008.

[43] I. Kuščer, Reciprocity in scattering of gas molecules by surfaces, Surf. Sci. 25 (1971) 225–237, http://dx.doi.org/10.1016/0039-6028(71)90244-5.

[44] N.F. Carnahan, K.E. Starling, Equation of state for nonattracting rigid spheres, J. Chem. Phys. 51 (1969) 635–636, http://dx.doi.org/10.1063/1.1672048.

[45] P. Resibois, M. De Leener, Classical Kinetic Theory of Fluids, Wiley, 1977.

[46] S. Homes, A. Frezzotti, I. Nitzke, H. Struchtrup, J. Vrabec, Heat and mass transfer across the vapor–liquid interface: A comparison of molecular dynamics and the Enskog–Vlasov kinetic model, Int. J. Heat Mass Transfer 242 (2025) 126828, http://dx.doi.org/10.1016/j.ijheatmasstransfer.2025.126828.

[47] S. Li, W. Su, B. Shan, Z. Li, L. Gibelli, Y. Zhang, Molecular kinetic modelling of non-equilibrium evaporative flows, J. Fluid Mech. 994, A16, http://dx.doi.org/10.1017/jfm.2024.605.

[48] S. Li, L. Gibelli, Y. Zhang, Non-equilibrium evaporation of Lennard-Jones fluids: Enskog-Vlasov theory and Hertz-Knudsen model, 2025, arXiv preprint arXiv:2508.15785.